PREDICTING THE RADIATIVE PROPERTIES OF CIRRUS CLOUDS

David L. Mitchell
Desert Research Institute
Reno, Nevada

1. INTRODUCTION

This paper will focus on new unpublished results, which are primarily concerned with validation of a new radiation treatment for cirrus clouds. The new radiation treatment is published in part in Mitchell and Arnott (1994), and will soon be published in Mitchell et al. (1995). The treatment of cirrus microphysics is discussed in Mitchell (1994) and in Mitchell et al. (1995).

The cirrus radiation treatment will be briefly summarized. Projected area-dimensional and mass-dimensional power laws were obtained for randomly oriented hexagonal columns and plates, bullet rosettes, and planar polycrystals such as side planes. These appear to be the most common crystal types in cirrus, the latter exhibiting extremely complex shapes. The area power laws for the spatial crystal shapes (rosettes and polycrystals) were obtained from ice particle formvar replicator data and 2D-C probe data. These mass and area power laws were used in the formulation of the absorption and extinction coefficients, based on anomalous diffraction theory (ADT), as described in Mitchell and Arnott (1994). The asymmetry parameter, g, was represented in terms of wavelength, λ, for each of these four ice particle shapes, where the size dependence of aspect ratio was accounted for regarding hexagonal crystals and rosette branches. For planar polycrystals, a second generation Koch fractal, with randomized tetraedic pyramid elements, was used as a surrogate for these very complex shaped crystals. Scattering phase function calculations for these and the other crystal types were performed in Germany by Andreas Macke, as described in Macke (1993; 1994).

In order to treat absorption and extinction by ice crystals, the "effective distance", D_e, which accounts for the absorption and extinction of radiation as it passes through an ice crystal, needed to be determined and parameterized. This distance accounts for the representative phase shift between waves transmitted through the crystal and parallel waves adjacent to the crystal. This phase shift produces the interference patterns, and the maxima and minima in the extinction efficiency for size parameters ($x = \pi D/\lambda$) < 30. Also, D_e is the "Beer's Law distance" over which absorption occurs. It is defined as $D_e = V/P$, where V is the ice crystal volume at bulk ice density, and P is the crystal's projected area. The method for parameterizing D_e into the extinction and absorption coefficients is described in Mitchell et al. (1995).

When parameterizing the extinction and absorption coefficients, two properties of an ice crystal population (i.e. size distribution) are conserved: (1) the D_e values and (2) the size distribution projected area. This accounts for the intuitive expectation that a photon interacting with an ice crystal branch (such

as a bullet rosette branch) does not experience an equivalent mass or area sphere, but "sees" only the branch. At the same time, the physical projected area of the size distribution is retained when converting the actual size distribution into ice spheres having D_e values equivalent to those of the ice crystals. The conversion to D_e equivalent spheres was necessary for obtaining an analytical formula from ADT for the extinction coefficient.

2. VALIDATION OF THE CIRRUS RADIATION TREATMENT: COMPARISON WITH LABORATORY MEASUREMENTS

Measurements of extinction efficiency (Q_{ext}) were made in a laboratory ice cloud over wavelengths in the thermal infrared. Details can be found in Arnott et al. (1994a;b). The ice cloud was produced from a supercooled water cloud at the top of a chamber by introducing a rod soaked in liquid nitrogen. Radiation was emitted from a 0.685 μm laser and a Fourier Transform Infrared Spectrometer (FTIR), covering a range from 2 to 18 μm. Sensors measured the attenuation of radiation from the dense ice cloud, which had an optical depth, τ, of around 1. The 0.685 μm laser gave a measure of the size distribution projected area, since for $x > 30$, $\tau \approx 2$ x (mean size distribution projected area) x L, where L is the path length (2.18 m) and τ is measured. The IR extinction efficiency is then measured as

$$Q_{ext,IR} = 2\tau_{IR}/\tau_{0.685\ \mu m} \quad . \qquad (1)$$

The ice cloud was sampled just below the laser beam by sucking ice crystals through a funnel and impacting them on a microscope slide, where they were video recorded. Assuming an optical depth of 1, a relative size distribution was generated, which is valuable in determining the mean ice crystal maximum dimension ($\bar{D}$). Unfortunately, ice crystals with $D < 15$ μm appear to be severely undersampled, due to their low collection efficiencies. However, the largest crystal sizes can be used to fit an analytical gamma distribution, which measured size spectra generally conform to (Mitchell 1994). From the gamma distribution fit to the larger ice crystal sizes, $\bar{D}$ was estimated. An example is shown in Fig. 1, where the measured size distribution is for columns grown at -7°C, and $\bar{D}$ for the gamma distribution fit was 7 μm.

Using the new radiation treatment for ice crystals, Q_{ext} was calculated theoretically for a size distribution of hexagonal columns, using the size distribution fit in Fig. 1 ($\bar{D} = 7$ μm). This is shown by the heavy solid curve in Fig. 2. The short dashed curves correspond to measured values of Q_{ext}, with ice cloud growth times accounting for the observed variability. As the cloud ages, $\bar{D}$ changes and the measured curves shift slightly. This same result was reproduced theoretically, where theory predicted the change in $\bar{D}$ was from about 6 to 8 μm. Thus, the behavior of Q_{ext} appears very sensitive to changes in $\bar{D}$. In fact, our treatment predicts that the minima in Q_{ext} virtually disappear, with $Q_{ext} \approx 2$, for $\bar{D} > 30$ μm.

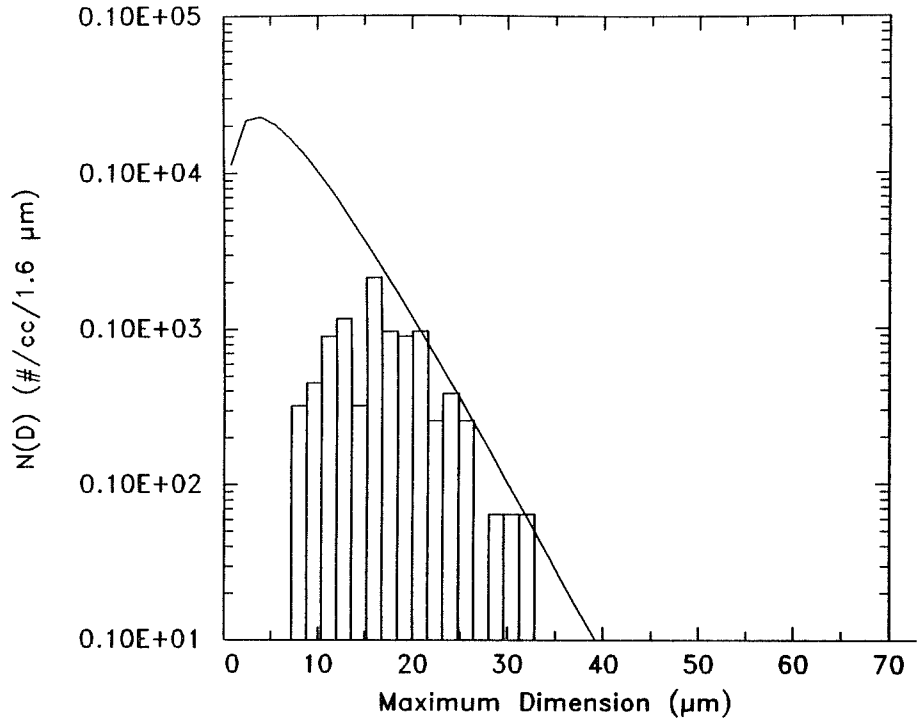

Fig. 1. Measured size distribution (histograms) for an ice cloud of hexagonal columns, grown at -5°C in a laboratory cold box. The gamma distribution fitted to the measured distribution for D > 15 μm has a mean maximum dimension of 7 μm.

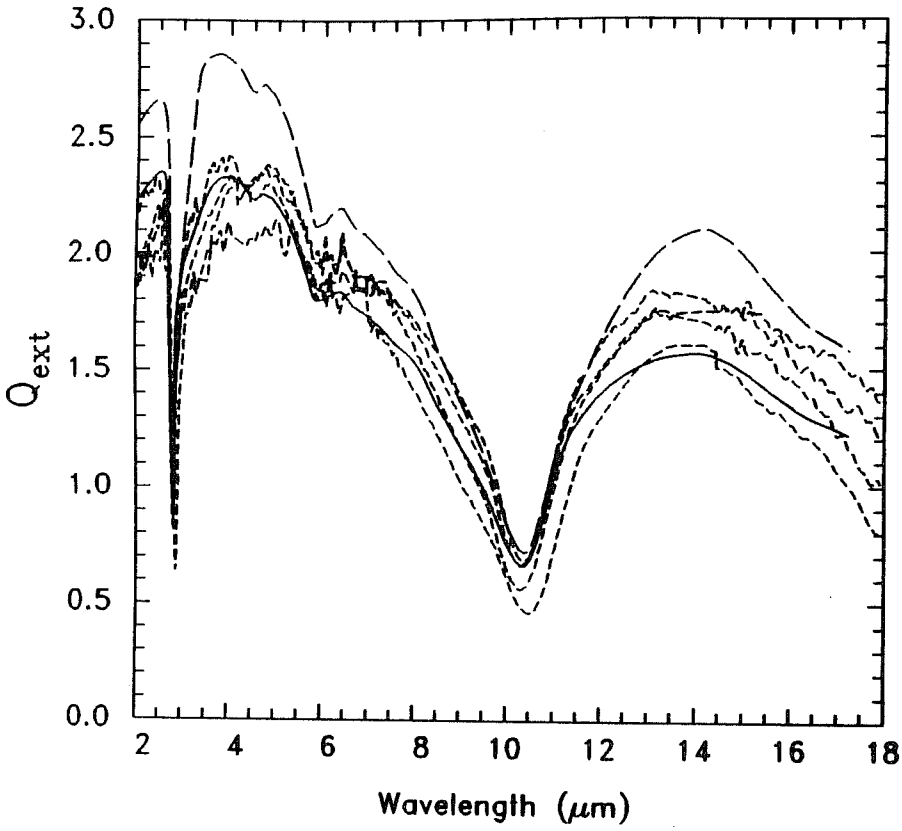

Fig. 2. Extinction efficiency measurements (short-dashed curves) for an ice cloud of hexagonal columns, corresponding to the size distributions in Fig. 1. The solid curve was predicted by the new cirrus radiation treatment, which is based on anomalous diffraction theory, while the long-dashed curve was based on MIE theory. The gamma distribution in Fig. 1 was used for both theoretical curves.

The long-dashed curve is based on MIE theory. This will be discussed more in Section 4.2. A similar comparison between lab measurements and theory was made when the ice cloud was composed primarily of hexagonal plates, and $\bar{D}$ was 14 μm. Agreement between theory and experiment in this case was equally as good as the case with columnar crystals.

The cause of the extinction minima near 2.8 μm and 10.3 μm are the result of the real part of the refractive index, n_r, approaching a value of 1.00. When $n_r = 1$, scattering due to refraction and reflection is minimized. Thus, the alteration of radiation transmitted through an ice crystal will be minimal, contributing little to extinction. Also, when $n_r = 1$, there is no phase lag for waves passing through the crystal, so there is no wave interference contribution to extinction. This leaves diffraction and absorption to contribute to Q_{ext} at the extinction minima. With just these two processes, $Q_{ext} \approx 2$ when absorption is strong and $D >> \lambda$. But as the particle size becomes comparable to or smaller than the wavelength, the ability of the particle to scatter radiation via diffraction decreases, and absorption becomes the dominant contributor to Q_{ext}. As ice crystal size decreases, absorption changes from an area dependence to a mass dependence (or D_e dependence), and the absorption efficiency, Q_{abs}, decreases. This is why the minima for Q_{ext} can be < 1, even though the *imaginary* index of refraction is substantial at 2.8 and 10.3 μm. This complex dependence of the extinction minima on the above phenomena puts theory to a rigorous test.

3. VALIDATION OF THE CIRRUS RADIATION TREATMENT: COMPARISON WITH FIELD MEASUREMENTS

In this section, a simple analytical two-stream model formulation is used (Mitchell et al. 1995), to determine whether the radiative properties predicted from observed microphysics in cirrus case studies compare favorably with the observed radiative properties. Predicted reflectances are integrated over all angles of incidence and reflection, and are thus hemispheric averages. Reflectances were calculated from the analytical two-stream formulation the Sagan and Pollack (1967), which was found to be accurate to within a few percent when compared to exact solutions for limiting cases. Emissivities were calculated using the zero scattering approximation, which should be accurate to within at least 5%. Albedo vs. emissivity curves were generated by assuming an ice particle shape and mean size, and then varying the IWP. Albedo calculations were based on wavelengths in the visible and near IR, while broadband emissivities were calculated over wavelengths from 5 to 50 μm.

To compare observed radiative properties with those derived theoretically from observed microphysics, data sets were obtained from the studies by Stackhouse and Stephens (1991), which contained FIRE I data, and Paltridge and Platt (1981). Complementary microphysical data was obtained from Heymsfield et al. (1990) regarding the FIRE I data. These data sets are unique in that the research aircraft measured

broadband emittance, solar albedo, and ice particle size spectra for the same region of cloud. The latter made it possible to estimate $\bar{D}$ and the ice water path (IWP). The FIRE I data also contained information on ice particle shape, an important parameter in this radiation treatment.

3.1 **FIRE case study of 28 October 1986**

We will first discuss the FIRE I case study of 28 October, 1986. The cirrus deck on this day consisted of two layers, an upper cloud sampled by the Sabreliner and a lower cloud sampled by the King Air. The lower cloud contributed most of the IWP. The median mass dimension in the upper cloud averaged about 300 μm, suggesting a mean maximum dimension ($\bar{D}$) in the upper cloud of about 100 μm (based on the dominate crystal shapes and an exponential size distribution). Similar analysis revealed that the $\bar{D}$ representative of the lower cloud was about 180 μm. The ice crystal shapes which dominated optical depth are as follows. Based on 2D-C probe data and ice crystals impacted on oil coated glass slides, the upper cloud was dominated by bullet rosettes and spatial polycrystals. Spatial polycrystals dominated the lower cloud, followed by rosettes. Some spatial polycrystals had extensions, typical of planar polycrystals, while a similar amount were reported to be compact and approximately isometric. The later type may have optical properties similar to short columns if crystal mass occupies relatively little volume.

Downward and upward total shortwave (0.3-3.0 μm) and longwave (4.0-50.0 μm) mean irradiances were measured by pyranometers and pyrgeometers, respectively. Hemispheric mean albedos and emittances calculated from these fluxes should provide for meaningful comparisons with corresponding predicted values. The zenith angle for the 28 Oct. case study was 61 degrees.

Reflectances and albedo tend to be weighted by the microphysics characterizing the upper cloud region. Theoretical emissivities should be comparable to measured emittances, although downward emittances are weighted by the microphysics lower in the cloud, and the converse is true for upward emittances. Emissivities were based on a mean cloud temperature of -38°C, averaged over both upper and lower cloud regions. Like the theoretical values, measured albedos and emittances shown are for the cloud only, without contributions from the surface (P. Stackhouse, private communication).

Predicted cloud albedo is plotted against emissivity in Fig. 3 for the ice particle shapes indicated, assuming a mean ice particle dimension of 100 μm. Data points indicated by circles correspond to the 28 Oct. FIRE I case study. Figure 4 is similar, except a $\bar{D}$ of 180 μm was used. These sizes roughly correspond to $\bar{D}$ in the upper and lower cloud, respectively. It is seen that most of the points are bracketed by the curves for columns, rosettes and/or planar polycrystals. As noted, the dense, compact, spatial crystals observed may behave optically more like columns. Thus, these theoretical curves are consistent with both the sizes and shapes observed during this case study.

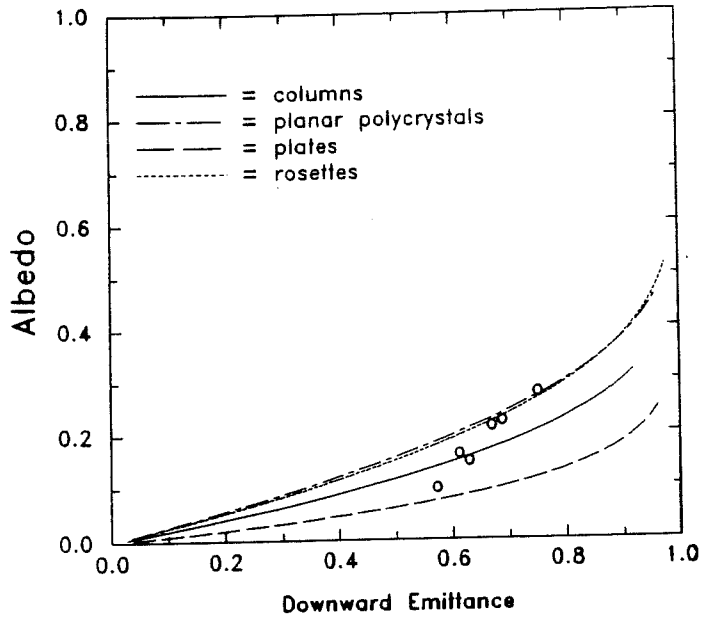

Fig. 3. Solar albedo vs broadband downward emittance curves, based on the new treatment of radiation, for different ice crystal shapes. Shown for comparison are measured values (circles) obtained during the 28 October 1986 FIRE I cirrus case study. The mean ice crystal size used in the model was 100 μm, where the size distribution form was exponential. The mean ice crystal size (D) observed in the upper cirrus cloud on 28 October was about 100 μm.

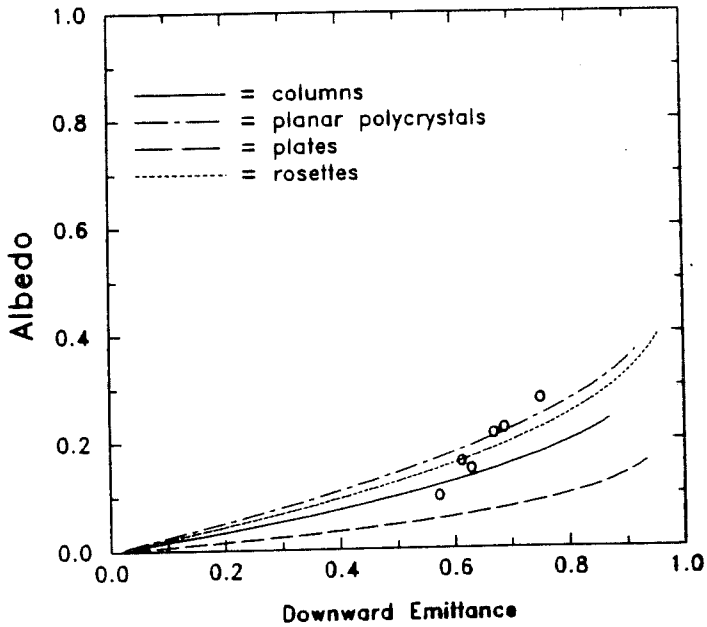

Fig.4. Same as Fig. 1, except the curves are based on a D of 180 μm, which was representative of the lower cirrus cloud on 28 October 1986.

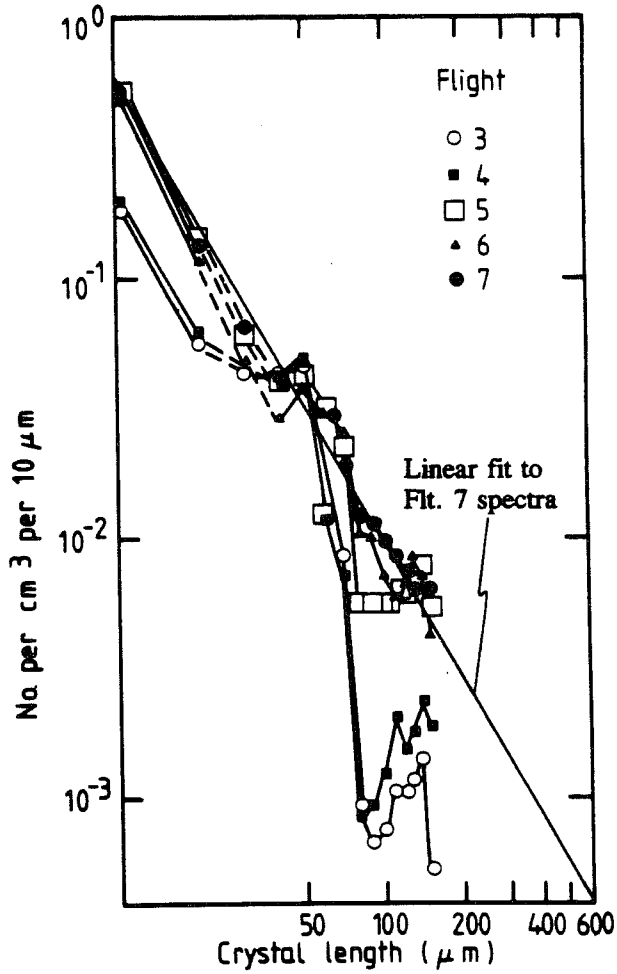

Fig. 5. Measured and parameterized size distribution for Flight 7, as reported in the cirrus cloud study by Paltridge and Platt (1981).

3.2 Paltridge and Platt cirrus case study

Another microphysics/radiation cirrus case study was conducted in 1979 by Paltridge and Platt (1981). The most microphysically uniform cirrus deck for which the most measurements were made was sampled during Flight 7. We chose the Flt. 7 case study of 27 March 1979 to compare with our radiation treatment. The cirrus deck was 1.8 km thick. The zenith angle the radiation measurements were made was about 40 degrees. Albedos and emittances were derived from hemispherical fluxes of the entire spectrum of solar and terrestrial radiation, respectively. The albedo and emissivity calculations here are also based on such broadband, hemispheric averages, making the comparisons meaningful.

No measurements of ice crystal shape were made during the Paltridge and Platt study, although ice size spectra were measured during five flights using a 1-D Knollenberg cloud probe, which measured ice particles from 5 to 150 μm in 10 μm steps. All particles measured were assumed to be randomly oriented hexagonal columns. The probe analysis procedure assumed random orientation and estimated column lengths which were greater than the measured sizes. However, its quite possible that the ice consisted of spatial ice crystals (3-dimensional), where their true maximum dimension was the measured size. There was remarkably little variation of the size spectra with height within the cloud. The size spectra for Flt. 7 is shown in Fig. 5 in log-log space by the solid circles. The straight line approximates the form of the size distribution. From the slope and intercept of this line, the size distribution was approximated as

$$N(D) = AD^B , \qquad (2)$$

where A = 0.002815, B = -1.7527, cm units. Assuming the distribution form continues past 10 μm down to 1 μm size or less (a reasonable assumption as demonstrated in Knollenberg et al. 1993), $\bar{D}$ was determined from (1) as 9.66 μm.

A $\bar{D}$ value of 10 μm was assumed to generate the IWP/albedo/emittance relationships. Theoretical values of albedo vs emittance are compared with measured values, given by the + marks, in Fig. 6. Measured and theoretical values agree well for all of the four ice crystal shapes. The lower solid curve was generated for columns by treating the absorption and extinction cross-sections in accordance with MIE theory, but treating the phase function (asymmetry parameter in this case) the same in each of these column simulations. This will be explained in more detail below.

4. REASON FOR AGREEMENT BETWEEN MEASUREMENTS AND THEORY

Many investigators have attempted to explain the above observed relationships, and other observations regarding cirrus-radiation interactions, with only partial success. For instance, the parameterization for hexagonal columns by Fu and Liou (1993) predicted albedo/emittance curves which exhibited only a weak dependence on effective particle size, showing less dispersion than the FIRE I data. No one has explained until now the albedo/emittance measurements of Paltridge and Platt, shown in Fig. 6.

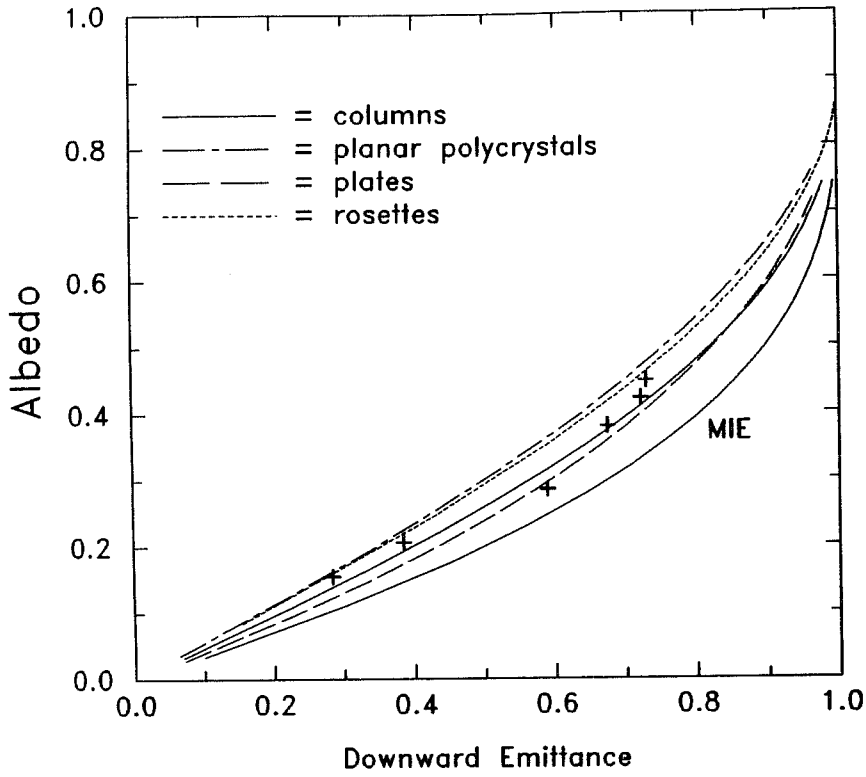

Fig. 6. Albedo-emittance data (+) from the cirrus cloud sampled by Paltridge and Platt during Flt.7. Mean ice particle sizes based on measurements were estimated to be about 10 μm. The theoretical curves shown for various ice crystal types were based on $\bar{D}$ = 10 μm. Curves for hexagonal columns were generated from the ADT treatment (upper solid) and MIE theory (lower solid curve).

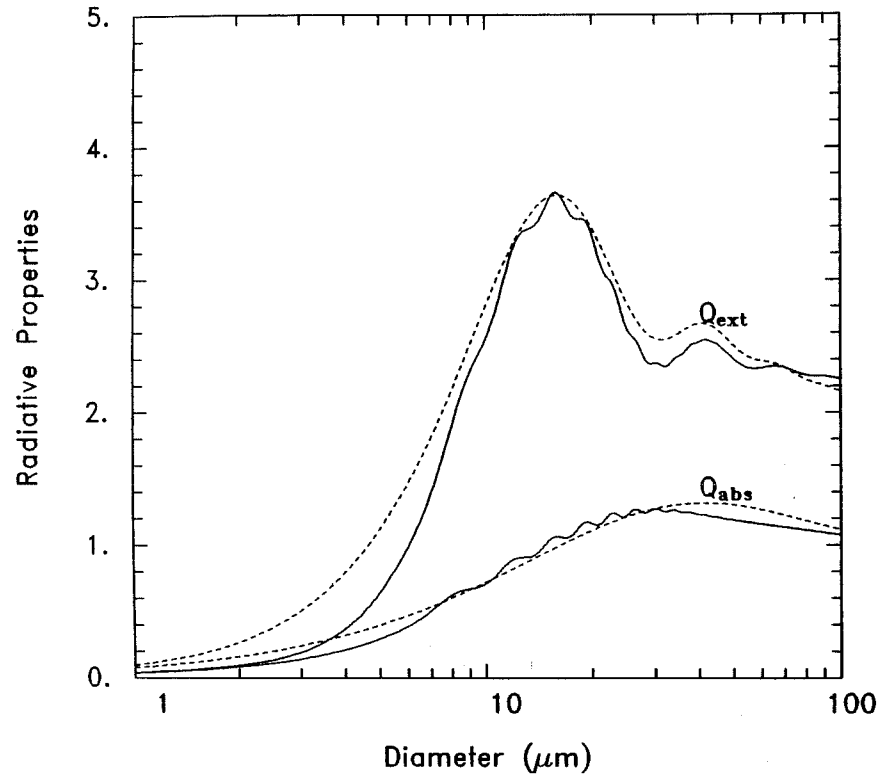

Fig. 7. Extinction and absorption efficiencies predicted by MIE theory (solid curves) for ice spheres, where λ = 15 μm, n_r = 1.6 and n_i = 0.1. The dashed curves were predicted by the modified ADT, as described in the text. The one-to-one correspondence of the ripple structure between extinction and absorption curves is evident.

There are two primary reasons why this radiation scheme predicts the observed radiative properties of ice clouds: (1) The average distance a photon experiences as it passes through an ice crystal is adequately represented, and (2) the absorption and extinction cross-sections are treated appropriately. The first reason has already been discussed. The second reason is more elusive, and deals with some very subtle physics. In this section, we will deal only with the second reason.

The absorption cross-section of a sphere, predicted by MIE theory, can be greater than the physical cross-section. Anomalous diffraction theory (ADT) predicts that the radiation absorbed by a particle cannot exceed the particles physical cross-section (or projected area). But why are the two theories different in this respect, and which theory is most applicable to non-spherical particles? To explore this issue, a method was developed to make ADT act like MIE theory, predicting similar absorption and extinction cross-sections.

4.1 Modification of ADT

The absorption efficiency predicted by ADT was modified to yield results for ice spheres similar to those predicted by MIE theory. Since the physics behind ADT, which is a simplification of MIE theory, is well understood, the modifications made to ADT may help reveal the physics accounting for the differences between ADT and MIE theory. If these differences are better understood, then we can ask whether the processes creating these differences are applicable to non-spherical particles. We begin by modifying the absorption efficiency, Q_{abs} .

An objective in modifying ADT to fit MIE theory was to do so in a way which allows the absorption and extinction efficiencies to be integrated over the ice particle size distribution, rendering analytical expressions for the absorption and extinction coefficients, β_{abs} and β_{ext}. The simplest approach possible was sought. These objectives led to a somewhat intuitive approach, where the correction terms required for modifying Q_{abs} were reduced to two. The first term, C_1, empirically adjusts ADT for spheres to account for the contribution of internal reflection and refraction to Q_{abs}. ADT treats radiation as passing straight through the particle. The second term, C_2, accounts for the absorption cross-section being greater than the physical projected area for strong absorption, when $D \approx \lambda$. The absorption efficiency, modified to act like Q_{abs} predicted by MIE theory for ice spheres, is then given as

$$Q_{abs,mod} = (1 + C_1 + C_2)Q_{abs,ADT} \ . \qquad (3)$$

The first term was formulated as

$$C_1 = a_1(1 - Q_{abs,ADT}) \ ,$$

or

$$C_1 = a_1 \exp(-8\pi n_i D/3\lambda) , \qquad (4)$$

where n_i is the imaginary part of the refractive index, and $a_1 = 0.25$. Equation (3) was formulated by noting the extra contribution of internal reflection and refraction to absorption would diminish as $Q_{abs,ADT}$ increases, which has a limiting value of 1. Naturally, there can be no such contribution when no radiation can pass through the particle (i.e. absorption depends only on projected area). The coefficient a_1 was determined empirically by examining differences between ADT and MIE values of Q_{abs}, primarily at x values in the near IR where the contribution of C_2 was minimal.

In addition to internal reflection and refraction, there is another, less understood process, which contributes to absorption for ice spheres. This process dominates over internal reflection and refraction by a wide margin when absorption is strong (such as in the thermal IR), and has a maximum when $D \approx \lambda$. This process, represented by C_2, appears to involve the capture of photons by a sphere which are not on a "collision trajectory" regarding the sphere's physical cross-section. The absorption efficiency for strong absorption reaches a maximum (> 1) when $D \approx \lambda$. Considering the photon as a particle, the increased cross-section might be explained through the Heisenberg uncertainty principle. This topic, though extremely fascinating, is beyond the scope of this paper. Suffice it to say that grazing photon trajectories, which do not physically collide with the sphere, can be captured anyway. The captured photon then appears to propagate as a surface wave, as discussed in van de Hulst (1981). A portion of the incident wave is preferentially captured as a surface wave at the first resonance peak in Q_{ext} when $D/\lambda_m = 1$, where λ_m is λ within the medium (van de Hulst 1981, p. 281; $\lambda_m \approx \lambda/n_r$). Other resonance peaks occur in increments of about 0.8 x, where $x = \pi D/\lambda$. Grazing photons appear to be preferentially captured as surface waves when λ corresponds to a resonance peak. Once captured as a surface wave (which propagates along the sphere's surface, circling the sphere), the photon can be absorbed into the particle, or "sprayed" away as a departing wave (contributing to scattering). The degree that the surface wave contributes to absorption and extinction depends on the real and imaginary parts of the refractive index.

The enhancement of the absorption cross-section through the capture of grazing photons occurs over a region that can be crudely estimated with a gamma function, which approximates a bell-shaped curve. This function was chosen since it was integratable and gave a good fit. The correction term for grazing photon capture is given as

$$C_2 = a_2 x^m \exp(-\epsilon x) , \qquad (5)$$

where $x = D/\lambda$, $m = 0.5$, and

$$a_2 = (0.7393\ n_r - 0.6069)/[x_{max}^{m} \exp(-m)] , \quad (6)$$

$$x_{max} = m/\epsilon , \quad (7)$$

$$\epsilon = a_1 + 0.6\ [1 - \exp(-8\pi n_i/3)]^2 . \quad (8)$$

The term x_{max} indicates the x value where this absorption enhancement effect is greatest. Although the location of x_{max} may be determined theoretically in the future, x_{max} is currently estimated empirically via (7) and (8). The magnitude of this absorption enhancement at x_{max} was also determined empirically in the same manner, by comparing $Q_{abs,ADT}$ with $Q_{abs,MIE}$ from $\lambda = 2\ \mu m$ to $100\ \mu m$ for about 25 wavelengths, with D ranging from $10\ \mu m$ to $1000\ \mu m$. Wavelengths were studied where the difference between $Q_{abs,ADT}$ and $Q_{abs,MIE}$ was almost entirely due to C_2, which yielded values of a_2. Equation (6) represents these measured values to within $\pm$ 0.03, suggesting that the magnitude of this effect depends essentially on n_r.

Next, $Q_{ext,ADT}$ was modified to act like Q_{ext} predicted by MIE theory for ice spheres. This was done in almost the same way as $Q_{abs,mod}$ regarding grazing photon capture:

$$Q_{ext,mod} = (1 + C_3)Q_{ext,ADT} , \quad (9)$$

where

$$C_3 = a_3\ x^m \exp(-\epsilon x) , \quad (10)$$

$$a_3 = (n_r^{2/3} - 1)/[x_{max}^{m} \exp(-m)] . \quad (11)$$

Alternatively, the numerator in (11) can be replaced with $(n_r - 1)/1.5$, with similar accuracy (slightly better at low n_r, worse at high n_r). These formula are most applicable for $\lambda \leq 45\ \mu m$, $D > 10\ \mu m$, and $1.1 < n_r < 1.8$. These conditions are satisfied at solar and most terrestrial radiation wavelengths, and for most ice particle sizes found in cirrus clouds. Under these conditions, single particle errors are generally $< 10\%$. However, when calculating absorption and extinction coefficients from these formula over a size distribution, deviations from MIE theory may be $<< 10\%$, since errors tend to cancel. For β_{abs} and β_{ext}, the above limits for D and λ could be extended considerably with errors still $\leq 10\%$.

One of the most significant results of this exercise is the close similarity between C_2 and C_3 - only their maxima at x_{max} differ. This suggests that the same physical process is responsible for the correction of

both $Q_{abs,ADT}$ and $Q_{ext,ADT}$ in the region where $D \approx \lambda$. As mentioned above, this process may be the capture of grazing photons in the form of surface waves. The coupling of Q_{abs} and Q_{ext} through this process can be seen in Fig. 7, where $\lambda = 15$ μm, $n_r = 1.6$ and $n_i = 0.1$. The ripples in the curves for $Q_{abs,MIE}$ and $Q_{ext,MIE}$ (solid curves) are seen to correspond exactly, indicating they are the result of the same process. These ripples in the interference patterns for Q_{ext} are believed to be due to surface wave resonance effects (van de Hulst 1981). If n_r is increased (at constant n_i), the ripple amplitudes increase for both absorption and extinction, as indicated by (5), (6), (10), and (11). If n_i is increased (at constant n_r), the ripple peaks attenuate and eventually disappear, since absorption of surface waves reduces scattering from wave resonance effects.

The dashed curves in Fig. 7 were predicted by (3) and (9). Without these corrections, at $D = 15$ μm, $Q_{abs,ADT}$ was 45% lower than $Q_{abs,MIE}$, and $Q_{ext,ADT}$ was 27% lower than $Q_{ext,MIE}$. The modified ADT presented here should serve as a reasonable surrogate for MIE theory regarding cloud droplets and ice particles, and may find use in situations demanding computational efficiency in calculating β_{abs} and β_{ext}, for which analytical formulae can be derived.

4.2 Implications for non-spherical particles

Now that we have some understanding of the differences between ADT and MIE theory, we can ask whether these physical differences are relevant to non-spherical particles. Surface waves and associated resonance structures need a continuous surface on which to propagate (van de Hulst, 1981, p. 367; Barber, private communication). Once a discontinuity is introduced, such as 60° or 90° angles found in ice crystals, the resonance structure is destroyed. Thus, surface wave resonance structures are not supported by irregular particles. Prolate and oblate spheroids with only small deviations from spherical geometry can still support these resonances to a lesser degree, and resonance effects occur with cylinders (Barber and Hill 1990).

For the first time, this combination of theory with the experimental results in Arnott et al. (1994; 1995) demonstrates the appropriateness of ADT for predicting the scattering and absorption properties of irregular particles in the infrared, and the inappropriateness of using MIE theory. The MIE theory curve in Fig. 2 was produced using β_{ext} calculated from (9), using the same size distribution of equivalent D_e spheres as the ADT result. The MIE parameterization probably overestimates the MIE curve for $\lambda > 13$ μm, although at shorter wavelengths, the MIE curve clearly exceeds the observations. The difference between ADT and MIE theory in the IR appears to be the capture of grazing photons, which manifest as surface wave resonance structures when $D \approx \lambda$. These resonance structures diminish with decreasing n_r, which is why the MIE curve agrees with the observations in the extinction minima. These results lend experimental evidence that the contribution of surface waves to scattering and absorption occur strongly only for spheres or particles with quasi-spherical, continuous surfaces.

The calculation of the MIE curve for columns in Fig. 6 was done in the same way as the ADT calculation for columns, except that (3) and (9) were used in calculating β_{abs} and β_{ext}, and the other radiative properties derived from these. The same size distribution of D_e equivalent spheres and the same asymmetry parameter value was used in the MIE and ADT simulation for columns. Previous investigators have used equivalent area or volume spheres, which are considerably larger than D_e spheres, which would make the MIE curve for columns even lower. The MIE curve shown here exhibits a poor fit to the data primarily because MIE theory predicts photons of grazing incidence are captured, and NOT because of any deficiencies in the scattering phase function.

In conclusion, both a laboratory study and a field study have shown that MIE theory is not appropriate to represent the radiative effects of non-spherical particles, due to the extra physics which is valid only for spherical particles. Moreover, a simple treatment of radiative properties, based on anomalous diffraction theory (which could be carried out on a calculator), predicted radiative properties for ice clouds from the observed microphysics which agreed well with the observed radiative properties. This was true for the laboratory study and the two field studies.

Acknowledgments: Stimulating conversations with Dr. Pat Arnott at DRI, and Dr. Georg Witt at Stockholm University, are gratefully acknowledged, and added to the quality of this paper. Dr. Arnott is also thanked for the use of his laboratory data. This work was funded in part by the NOAA Climate and Global Change Program as an aspect of the Global Energy and Water Cycle Experiment (GEWEX). Partial funding was also provided by the U.S. Dept. of Energy's Atmospheric Radiation and Measurement Program (ARM).

5. REFERENCES

Arnott, W.P., Ya.Y. Dong and J. Hallett, 1994: Extinction efficiency measurements in the thermal IR of laboratory ice clouds. *Preprints, Eighth Conference on Atmospheric Radiation*, AMS, Nashville, Tennessee, January 23-28, 1994, 304-306.

Arnott, W.P., Ya.Y. Dong and J. Hallett, 1995: Extinction efficiency in the IR (2μm to 18 μm) of laboratory ice clouds: Observations of scattering minima in the Christiansen bands of ice. *J. Appl. Opt.*, January issue.

P.W. Barber and S.C. Hill, 1990: Light Scattering by Particles: Computational Methods. World Scientific, New Jersey, 261 pp.

Fu, Q., and K.N. Liou, 1993: Parameterization of the radiative properties of cirrus clouds. *J. Atmos. Sci.*, **50**, 2008-2025.

Heymsfield, A.J., K.M. Miller and J.D. Spinhirne, 1990: The 27-28 October 1986 FIRE IFO cirrus case study: Cloud microstructure. *Mon. Wea. Rev.*, **118**, 2313-2328.

Knollenberg, R.G., K. Kelly, and J.C. Wilson, 1993: Measurements of high number densities of ice crystals in the tops of tropical cumulonimbus. *J. Geophys. Res.*, **98**, 8639-8664.

Macke, A., 1993: Scattering of light by polyhedral ice crystals. *Appl. Opt.*, **32**, 2780-2788.

Macke, A., 1994: Scattering of light by irregular ice crystals in three-dimensional inhomogeneous cirrus clouds. *Preprints, Eighth Conference on Atmospheric Radiation*, AMS, Nashville, Tennessee, January 23-28, 1994, 304-306.

Mitchell, D.L., 1994: A model predicting the evolution of ice particle size spectra and radiative properties of cirrus clouds. Part I: Microphysics. *J. Atmos. Sci.*, **51**, 797-816.

Mitchell, D.L., and W.P. Arnott, 1994: A model predicting the evolution of ice particle size spectra and radiative properties of cirrus clouds. Part II: Dependence of absorption and extinction on ice crystal morphology. *J. Atmos. Sci.*, **51**, 817-832.

Mitchell, D.L., A. Macke, S.K. Chai, Y. Liu, Y. Dong, and A. Heymsfield, 1995: A model predicting the evolution of bimodal size spectra and the radiative properties of cirrus clouds, with quantification of ice crystal shape and aggregation effects. Submitted to the *J. Atmos. Sci.*

Paltridge, G.W., and C.M.R. Platt, 1981: Aircraft measurements of solar and infrared radiation and the microphysics of cirrus cloud. *Quart. J. R. Met. Soc.*, **107**, 367-380.

Sagan, C. and J.B. Pollack, 1967: Anisotropic nonconservative scattering and the clouds of Venus. *J. Geophys. Res.*, **72**, 469-477.

Stackhouse, P., and G. Stephens, 1991: A theoretical and observational study of the radiative properties of cirrus: Results from FIRE 1986. *J. Atmos. Sci.*, **48**, 2044-2059.

van de Hulst, H.C., 1981: Light scattering by small particles. Dover Publications, Inc., 470 pp.